Freestanding Membranes of Cross-Linked Gold Nanoparticles: Novel Functional Materials for Electrostatic Actuators

Hendrik Schlicke,[†] Daniela Battista,[†,‡] Svenja Kunze,[†] Clemens J. Schröter,[†] Manfred Eich,[§] and Tobias Vossmeyer*,[†]

[†]Institute of Physical Chemistry, University of Hamburg, Grindelallee 117, 20146 Hamburg, Germany
[§]Institute of Optical and Electronic Materials, Hamburg University of Technology, Eissendorfer Strasse 38, 21073 Hamburg, Germany

Ⓢ *Supporting Information*

ABSTRACT: Their tunable electrical, optical, and mechanical properties make freestanding membranes of organically cross-linked gold nanoparticles (GNPs) interesting materials for applications in micro- and nanoelectromechanical systems. Here, we demonstrate the application of α,ω-alkanedithiol-cross-linked GNP membranes as electrostatically driven actuators. The devices were fabricated by depositing these membranes (thickness 29−45 nm) onto cylindrical cavities (diameter ~200 μm; depth ~8−15 μm), which were lithographically patterned in a SU-8 resist. Applying voltages of up to ±40 V across the membrane and the silicon substrate deflected the membranes by several hundreds of nanometers, as measured by atomic force microscopy, confocal microscopy, and interferometry. A simple electrostatic model, which takes into account the membranes' mechanical properties, was used to interpret the experimental data.

KEYWORDS: *freestanding, membrane, gold, nanoparticle, MEMS, NEMS, actuator, electrostatic*
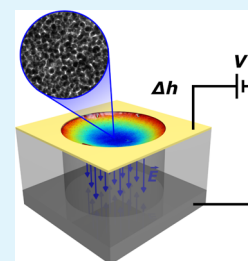
Composite materials containing metal or semiconductor nanoparticles are of considerable interest for the fabrication of micro- and nanoelectromechanical systems (MEMS/NEMS). Their electronic, magnetic, mechanical, and optical properties can be adjusted and tuned for specific target applications.[1−6] Further, these materials enable the cost-efficient fabrication of devices via laser writing, printing, and self-assembly techniques on various substrates.[7−11]

Recently, the mechanical properties of freestanding membranes comprised of ligand-stabilized gold nanoparticles (GNPs),[12,13] cross-linked GNPs,[14] or polymer/GNP composites[15] have been studied in different laboratories using atomic force microscopy (AFM) indentation or micro bulge tests. These investigations showed that GNP membranes are mechanically surprisingly robust. Furthermore, thermally excited and piezo-driven resonators based on GNP monolayers have been demonstrated, and their possible application as sensors has been proposed.[16] However, electrostatic actuation of such GNP membranes has not been demonstrated, so far, although this mode of actuation is a fundamental and widely used operating principle in MEMS.

The focus of our present work is on composite membranes of alkanedithiol (ADT)-cross-linked GNPs with thicknesses in the 20−100 nm range, which were fabricated via facile layer-by-layer spin-coating. The mechanical stability of these membranes allows for their transfer from their initial substrates onto various 3d microstructures to produce freestanding membranes.[17] This was demonstrated in a recent study, in which we investigated the material's elastic and viscoelastic properties via AFM bulge tests and measured a Young's modulus of ~2.5 GPa for 1,9-nonanedithiol-cross-linked GNP membranes.[14] In principle, the unique mechanical, optical, and charge-transport properties of GNP composites can be tuned by adjusting the particle size and shape or the size and structure of the cross-linker. For example, because charge transport in these membranes relies on thermally activated tunneling, the conductivity can be tuned over several orders of magnitude simply by using different length ADT linkers to tune the interparticle distances.[17−19] By using conjugated dithiocarbamate cross-linkers, it was even possible to yield metallic conductivity.[20] In addition, such tuning of the conductivity is accompanied by significant shifts of the plasmon absorbance band in the visible and near-IR spectral ranges. Current studies in our group investigate the influence of the cross-linker's size and structure on the mechanical properties of GNP membranes. Altogether, their tunable electronic, optical, and mechanical properties make GNP membranes a highly promising novel material for MEMS/NEMS applications.
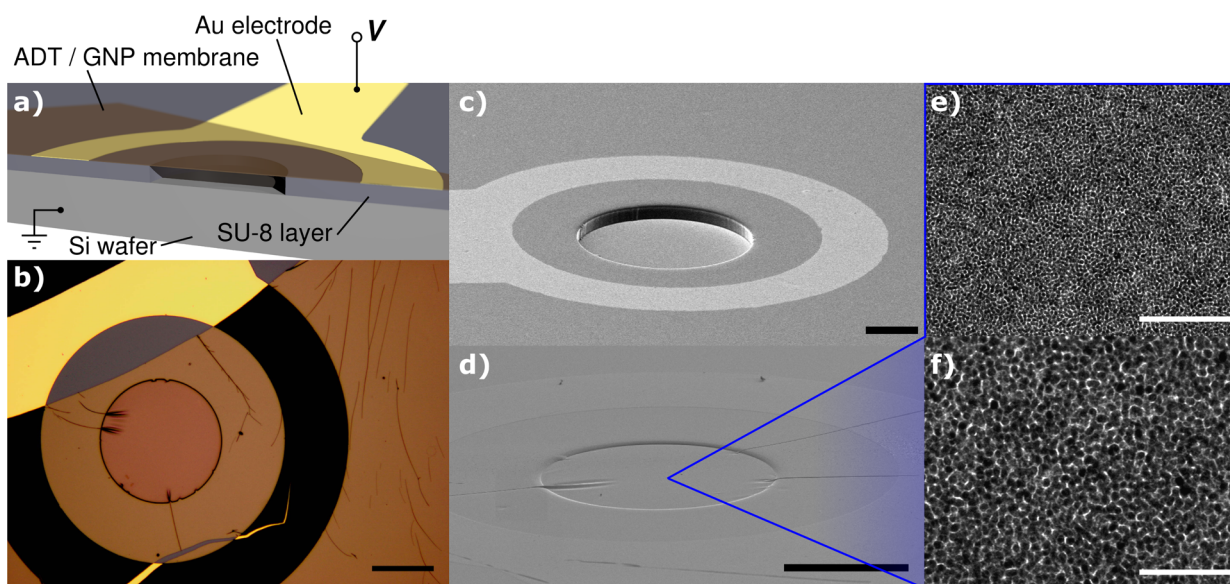
In this study, we present an electrostatic actuator exploiting the flexibility and conductivity of a GNP membrane as a functional material. To the best of our knowledge, this is the first demonstration showing electrostatic actuation of a conductive GNP membrane.

In principle, a freestanding section of a dithiol-interlinked GNP membrane, which acts as one electrode, is brought into close proximity to a silicon wafer representing the back electrode. By application of a potential difference, the elastic

Figure 1. (a) Schematic showing a cross-sectional view of the electrostatic actuator with an ADT-cross-linked GNP membrane deposited onto the ring-shaped top electrode. (b) Representative optical micrograph of such an electrostatic actuator. Scale bar: 100 μm. (c) SEM micrograph of the 3d-microstructured SU-8 resist having a cylindrical cavity with a ring-shaped top electrode. Scale bar: 60 μm. (d) SEM micrograph of an electrostatic actuator with a deposited 6DT-cross-linked GNP membrane spanning the cylindrical cavity. Scale bar: 100 μm. (e and f) Representative TEM micrographs of a 6DT-cross-linked GNP membrane. Scale bars: 100 and 50 nm, respectively.

membrane is deflected toward the latter by electrostatic forces resulting from opposite charging. Figure 1a schematically depicts a cross-sectional view of the electrostatic actuator. A SU-8 layer having a circular cavity equipped with a ring-shaped gold electrode was microfabricated on a doped silicon wafer (Figure 1c), and subsequently an ADT-cross-linked GNP membrane was deposited onto the 3d structure and remained freestanding above the microcavity (Figure 1b,d).

Initially, doped silicon substrates with a native oxide layer (p/B-doped, 1−10 Ω cm) were used as back electrodes, while in later experiments, doped silicon wafers (n/Sb-doped, 0.005−0.025 Ω cm; p/B-doped, <0.005 Ω cm) with a thermally grown oxide layer (~300 nm) were introduced. The thicker oxide layer enabled better electric insulation and, hence, suppressed parasitic direct-current conductance of the ideally purely capacitive device. Because of the low thickness of the oxide layer, its influence on the overall capacitance of the device is negligible. In the first fabrication step, a layer of SU-8 was deposited onto the back-electrode material by spin-coating. Photoresist layer thicknesses of ~8−15 μm were obtained by adjusting the spinnig frequencies. SU-8 is a nonconductive[3] negative-tone photoresist with high chemical and mechanical stability prevalently used for the fabrication of relief structures in MEMS.[21,22] The SU-8 layer was patterned through standard photolithography, yielding cylindrical cavities with a diameter of ~200 μm and a depth of ~8−15 μm, determined by the layer thickness. In the second step, the ring-shaped electrode structure was prepared on top of the SU-8 relief structure by patterning a sacrificial, second photoresist layer (AZ nLOF 2070) with a negative image of the electrode structure. Afterward, a ~100-nm-thick gold layer was deposited by thermal evaporation and the sacrificial photoresist layer was dissolved, baring the electrode by lifting off the gold layer from resist-coated areas. A ring-shaped electrode geometry around the cavity was chosen because it ensures a constant electrical potential of the freestanding membrane area, even if the membrane should have parasitic electrical contact to the back

electrode somewhere outside the electrode ring (e.g., by unwanted deposition of the membrane at the edges of the substrate). Figure 1c shows a representative example of the 3d electrode structure. The microfabrication process is described in detail in the Supporting Information (SI).

ADT-cross-linked GNP films were prepared via deposition onto glass substrates by alternately spin-coating a heptanoic solution of 1-dodecylamine-stabilized GNPs with an average diameter of 3−4 nm and a methanolic solution of the dithiol cross-linker. Upon application of multiples of these deposition cycles, the layer thickness can be adjusted in the range of 20−100 nm.[17] The GNP films exhibited characteristic UV/vis absorption spectra featuring a pronounced plasmon band and ohmic charge-transport behavior with conductivities of around 0.1 S cm^{-1}.[17] Representative UV/vis spectra and IV data can be found in the SI. Transmission electron microscopy (TEM) micrographs of a (38 ± <1)-nm-thick 1,6-hexanedithiol (6DT)-interlinked GNP membrane transferred to a carbon-coated TEM substrate are depicted in Figure 1e,f and reveal the membrane's nanoscale granular morphology. Representative TEM images of the GNPs used for film preparation are provided in the SI.

Following deposition, the GNP films could be detached from their glass substrates by carefully immersing the latter into demineralized water (Millipore, 18.2 MΩ cm), leaving the former floating on the liquid's surface. Afterward, the membranes were transferred to the electrode structures by skimming them off the liquid−air interface. After settling to the relief structure, the freestanding section of the membrane often showed wrinkle patterns, as are visible in Figure 1b. When the optical micrographs of the freestanding membrane sections are compared to those obtained from membranes deposited on circular 100 μm apertures for bulge test experiments in an earlier study, there was no slack observable. The appearance resembled taut membranes, with positive residual stress in the low megapascal range.[14]
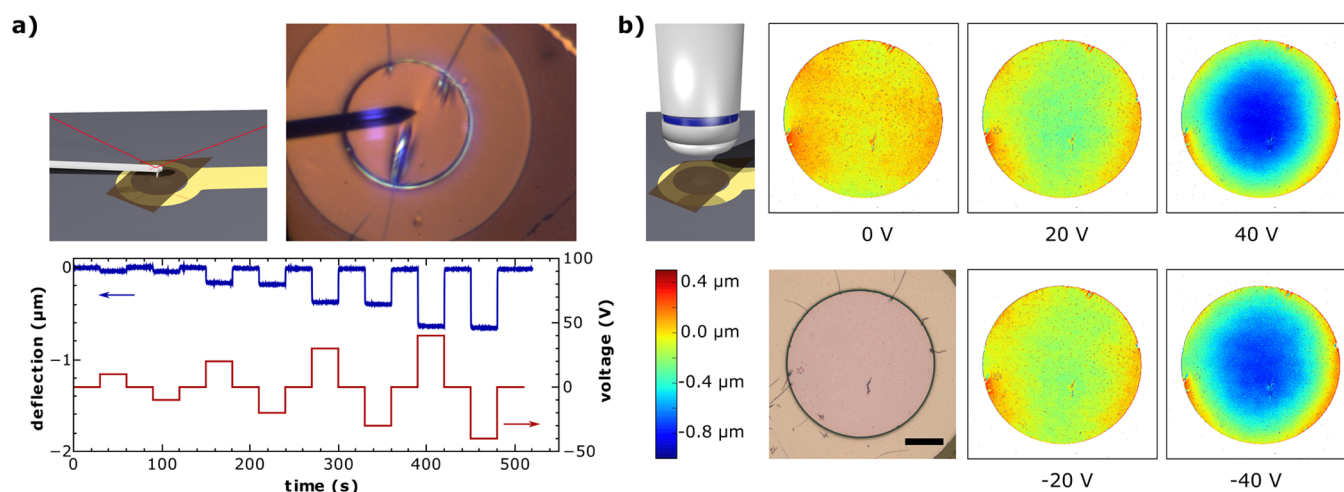
Figure 2. (a) Schematic of the AFM experiment used for probing the deflections of the actuator's 6DT-cross-linked GNP membrane (top, left). Optical micrograph acquired during the AFM experiment (cavity diameter ~200 μm; membrane thickness 45 nm; top, right). Recorded voltage and deflection traces (bottom). (b) Schematic of the actuator investigated by confocal microscopy (top, left). Optical micrograph of a 6DT-cross-linked GNP membrane (29 nm thickness) spanning the actuator's cylindrical cavity (bottom, left). Scale bar: 50 μm. Color-coded deflection maps recorded at different bias voltages as indicated (top and bottom).

Voltages of up to |V| = 40 V were applied to the membrane and back electrode to probe the devices' functionality. Figure 2a depicts a schematic and an optical micrograph of a 6DT/GNP-membrane-based actuator (device A) in an AFM setup. As determined by AFM, this membrane had a thickness of 45 ± 1 nm (see the SI).

The deflection of the membrane corresponding to different applied voltages was captured by AFM. As depicted in Figure 2a, an AFM probe (OSCM-PT, 0.5−4.4 N m^{-1}) was positioned close to the center on the membrane's surface in contact mode, and the membrane deflection was subsequently measured as a function of time. Voltages between −40 and +40 V were applied to the membrane in 30 s pulses, spaced by a 0 V delay of another 30 s. The figure shows time traces of the measured membrane deflection and the voltage applied to the sample. The deflection signal has a rectangular shape with steeply rising and falling edges, indicating a fast and reversible response of the actuator to the voltage signal. It should be noted that the measured deflections show no significant dependence on the bias direction. This is expected because the total charge and, hence, effective force only depend on the absolute value of the applied voltage. When the highest voltage of ±40 V was applied, the deflection of the membrane was ~0.6 μm.

An optical micrograph of another actuator (device B), based on a (29 ± 1)-nm-thick 6DT-cross-linked GNP membrane, is depicted in Figure 2b. The membrane shows fewer defects and wrinkles, and its deflection forced at different voltages was captured using a confocal microscope (Zeiss LSM700). Because this technique is a noncontact method, it is complementary to the AFM charactization, as described above. The obtained topographic images were leveled with respect to the measured height values of the SU-8 layer surrounding the freestanding membrane section and are presented in Figure 2b as color-coded deflection maps. The data indicate a pronounced deflection of the membrane center of ~0.2 and ~0.7 μm at applied voltages of |V| = 20 and 40 V, respectively. As in the AFM experiments, very similar deflections were measured when the bias direction was reversed. These results clearly demonstrate the functionality of the electrostatic actuators

comprising organically cross-linked GNP membranes as active components.

In order to interpret the voltage-dependent deflection of the GNP membranes, we consider the following simple model:

Ideally, the actuator presented in this work can be viewed as a parallel-plate capacitor, with the GNP membrane and the silicon wafer representing the two electrodes. The capacitance of the freestanding membrane section is given by $C = A\varepsilon/d$, where A is the freestanding membrane area, d is the distance separating the plates, and ε is the permittivity of the dielectric (air). Application of a bias voltage V to the device results in charging of the membrane and back electrode with a charge $|\pm Q| = CV$.

In a first approximation, the force F per unit area acting on the membrane can hence be obtained by taking into account the homogeneous electric field $E = Q/2A\varepsilon$ of one electrode screened by the charge density (Q/A) of the second electrode. Implication of the capacitance term for a parallel-plate capacitor yields eq 1.

$$\frac{F}{A} = \frac{Q}{A}E = \frac{Q^2}{2A^2\varepsilon} = \frac{C^2V^2}{2A^2\varepsilon} = \frac{\varepsilon V^2}{2d^2} \qquad (1)$$

Assuming a distance of $d = 10$ μm between the membrane and the back electrode, an applied bias voltage of $V = 40$ V, and a permittivity of $\varepsilon \approx \varepsilon_0$ for air, a force per area of $F/A = 71$ Pa acting on the membrane can be estimated. The force F is assumed to act along the electric field lines, i.e., orthogonal to the membrane's surface, pulling the membrane inward, into the cylindrical cavity.

While the electrostatic pressure acting on the membrane can be estimated by applying the simple electrostatic model outlined above, a relation describing the membrane deflection as a function of the bias voltage is more delicate to find. Here, we use an approach that is commonly applied for the interpretation of bulge test data. Bulge testing is a common procedure to study a material's elastic and viscoelastic properties. When this method is applied, a thin film of the material is deposited onto a substrate with a defined aperture and inflated by the application of varying overpressure. By

analysis of the resulting pressure−deflection data, information on the sample's mechanical properties is obtained.

A simple model describing the relationship between the applied pressure P and the central point deflection h of the bulged circular membrane is given by eq 2.[23] In good agreement with the experimental results,[14] it is based on the assumption of a spherical bulge geometry.

$$P(h) = \frac{8Yt}{3a^4}h^3 + \frac{4\sigma_0 t}{a^2}h \qquad (2)$$

In this equation, t is the film thickness, a is the aperture radius, Y is the biaxial modulus of the membrane material, and σ_0 its residual stress, which may be positive or negative for membranes in a taut or slack initial state, respectively. The above equation holds for small deflections ($h \ll a$) and low film thicknesses ($t \ll h$). The former constraint, which is fulfilled for our membranes measuring ∼200 μm in diameter and showing high nanometer-range deflections when biased with voltages up to 40 V, also implies that the membrane shows a fairly low curvature. Hence, the membrane's surface normals (in whose direction the force caused by an applied pressure would act) show only very little angular deviation from the electric field lines of an assumed homogeneous field applied between the almost flat membrane and the back electrode.

Therefore, we assume that the force per unit area acting on the membrane, originating either from the applied overpressure in a bulge test or from a homogeneous electric field as in the presented actuators, leads—under the above constraints and in a first approximation—to similar deflections. We, hence, replace the overpressure P by the voltage-dependent F/A term given in eq 1.

$$\frac{\varepsilon V^2}{2d^2} = \frac{8Yt}{3a^4}h^3 + \frac{4\sigma_0 t}{a^2}h \qquad (3)$$

It should be noted that this model neglects changes in the electric field originating from membrane movement and deformation, which can be significant in the case of larger deflections. Eventually, the above relationship between the applied voltage V and the central-point deflection h is based on several approximations, but it is expected to provide a useful description of increasing membrane deflections with increasing bias voltage, especially in the range of small deflections, with $h \ll d$, $h \ll a$, and $t \ll h$.

Figure 3a shows plots of the $V(h)$ data of actuators A and B depicted in Figure 2. To enable a more detailed analysis of the actuators' voltage−deflection behavior, the functionality of two further devices, C and D, was investigated. For these measurements, which were performed using an interferometric MEMS analyzer (Nanovibration Analyzer NA, SIOS Messtechnik GmbH), the membranes were deflected by applying voltages ranging from 0 to ±40 V and from 0 to ±30 V in steps of 2 V, respectively (see the SI). A clear nonlinear dependence is observed with deflections of up to several hundreds of nanometers for all devices. Also, fits of eq 3 to the data sets are depicted as solid lines. For these fits, a biaxial modulus for the 6DT-cross-linked GNP membranes of 8.9 GPa was implied, as determined by AFM bulge test experiments (see the SI). The membrane−wafer distance d was approximated as the SU-8 layer thickness, measured by profilometry or imaging of the SU-8 layer cross section by scanning electron microscopy (SEM), and the thickness t of the respective membrane was determined by AFM (Table 1 and the SI). The only remaining free-fit
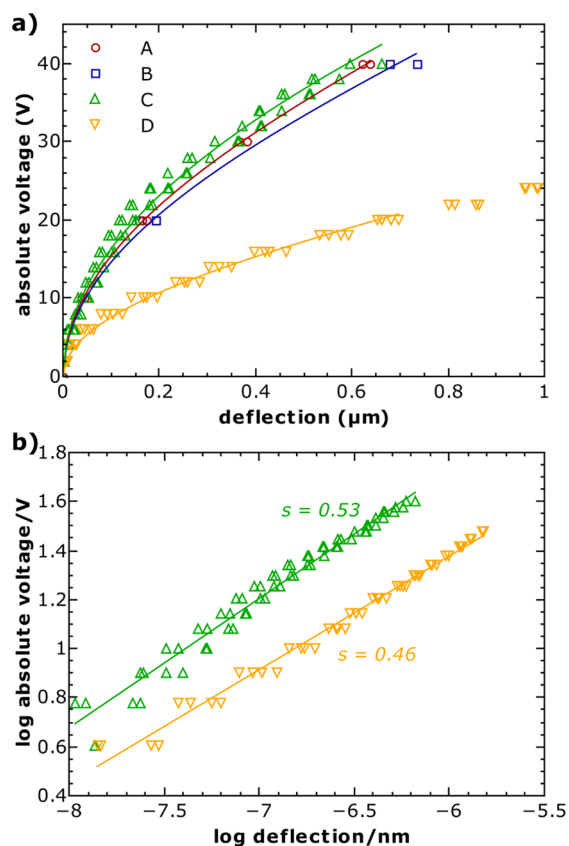
Figure 3. (a) Plots of the voltage−deflection relationship measured for the electrostatic actuator devices A and B shown in Figure 2a,b, as well as devices C and D, measured by interferometry. The solid lines represent fits of eq 3 to the respective data sets. The membranes had a diameter of ∼200 μm; other device parameters are presented in Table 1. (b) log/log plot of the $V(h)$ relationship found for devices C and D with linear fits (s denotes the slope of the fits).

Table 1. Device Parameters of Actuators A−D

device	membrane thickness t/ nm	SU-8 thickness d/ μm	residual stress σ_0/ MPa
A	45 ± 1	13	3.4
B	29 ± 1	15	3.6
C	37 ± <1	7.7	14
D	33 ± <1	7.6	3.3

parameter was the residual stress σ_0 of the freestanding membrane section. Because our model assumes a constant electric field, it is not applicable for the description of large deflections. Hence, data points with deflections in the range of >10% of the SU-8 layer thickness d were omitted for the fitting procedure. As seen in Figure 3a, the fit functions are in good agreement with the measured data and returned residual stress values ranging from 3.3 to 14 MPa (Table 1). Residual stress values in the low megapascal range are typical for freestanding membranes comprised of organically capped GNPs[13] or taut cross-linked GNP membranes[14] investigated previously via AFM nanoindentation or AFM bulge tests. We attribute the deviation of the residual stress value of actuator C to the fabrication process, which involves manual transfer of the membranes onto the 3d-structured substrates. It has been observed previously that the residual stress of cross-linked GNP membranes prepared by this procedure can scatter significantly.[14] As can be deduced from the device parameters listed

in Table 1, the strong deflection of device D compared to devices A and B at a given voltage is mainly due to the smaller electrode distance d. Compared to device C, the stronger response of actuator device D is essentially due to the much lower residual stress σ_0.

In eq 3, the first term takes into account the response of an initially relaxed membrane, whereas the second term accounts for the residual stress σ_0. With the parameters of the devices investigated and the maximum deflection considered for the fitting procedure, the residual stress term is about 1 order of magnitude larger than the first term. This dominance is also displayed by the square-root-like curvature of the $V(h)$ plots and is confirmed by plotting the data of devices C and D on a log/log scale (Figure 3b), returning slopes of 0.53 and 0.46, respectively. Thus, our model suggests that the voltage–deflection characteristic is qualitatively dominated by the residual stress of the membranes.

In conclusion, we presented the fabrication of electrostatic actuators based on organically cross-linked GNP membranes. 3d-microstructured ring electrodes were fabricated from SU-8 using standard photolithography, and the GNP films were deposited onto those structures, providing freestanding circular GNP membranes. When biasing the devices with voltages up to $|V| = 40$ V, central-point deflections of several hundreds of nanometers were measured using AFM, confocal microscopy, or interferometry. Qualitatively proving the functionality of these devices, the measured values are also in good agreement with estimations computed using a simple electrostatic model.

Our results highlight the capability of GNP membranes for future applications in MEMS/NEMS devices. Because of their conductive and flexible nature, they offer great potential for the fabrication of electrostatic actuators. By adjustment of the particle sizes as well as the size and structure of the cross-linker, these systems can be tailored regarding their mechanical, electrical, and optical properties to meet specific requirements for given applications. Current investigations aim at the excitation of similar devices by alternating voltage to enable electrostatically driven resonators, which are of interest for the development of ultrasensitive microgravimetric transducers. Here, the membranes' charge-transport mechanism, which is sensitive to strain,[24−26] could further be exploited for the facile electronic readout of the membranes' resonance frequency, resulting in all-electronic sensing devices.

ASSOCIATED CONTENT

Ⓢ Supporting Information

Characterization of the GNPs and substrate-supported GNP films, a detailed description of the lithographic processing methods and of the mechanical characterization of 6DT/GNP membranes by AFM bulge tests, and optical micrographs as well as voltage and deflection transients recorded during the interferometric measurements of devices C and D. The Supporting Information is available free of charge on the ACS Publications website at DOI: 10.1021/acsami.5b02691.

AUTHOR INFORMATION

Corresponding Author
*E-mail: tobias.vossmeyer@chemie.uni-hamburg.de.

Present Address
‡D.B.: Chemical Sciences and Technologies, University of Milano-Bicocca, Milano, Italy.

REFERENCES

(1) Damean, N.; Parviz, B. A.; Lee, J. N.; Odom, T.; Whitesides, G. M. Composite Ferromagnetic Photoresist for the Fabrication of Microelectromechanical Systems. *J. Micromech. Microeng.* **2005**, *15*, 29−34.

(2) Jiang, C.; McConney, M. E.; Singamaneni, S.; Merrick, E.; Chen, Y.; Zhao, J.; Zhang, L.; Tsukruk, V. V. Thermo-Optical Arrays of Flexible Nanoscale Nanomembranes Freely Suspended over Microfabricated Cavities as IR Microimagers. *Chem. Mater.* **2006**, *18*, 2632−2634.

(3) Jiguet, S.; Bertsch, A.; Hofmann, H.; Renaud, P. Conductive SU8 Photoresist for Microfabrication. *Adv. Funct. Mater.* **2005**, *15*, 1511−1516.

(4) Kandpal, M.; Sharan, C.; Poddar, P.; Prashanthi, K.; Apte, P. R.; Ramgopal Rao, V. Photopatternable Nano-Composite (SU-8/ZnO) Thin Films for Piezo-Electric Applications. *Appl. Phys. Lett.* **2012**, *101*, 104102.

(5) Lucas, T. M.; James, K. T.; Beharic, J.; Moiseeva, E. V.; Keynton, R. S.; O'Toole, M. G.; Harnett, C. K. Wavelength Specific Excitation of Gold Nanoparticle Thin-Films. *Appl. Phys. Lett.* **2014**, *104*, 011909.

(6) Tsai, K. L.; Ziaei-Moayyed, M.; Candler, R. N.; Hu, W.; Brand, V.; Klejwa, N.; Wang, S. X.; Howe, R. T. Magnetic, Mechanical, and Optical Characterization of a Magnetic Nanoparticle-Embedded Polymer for Microactuation. *J. Microelectromech. Syst.* **2011**, *20*, 65−72.

(7) Bai, Y.; Ho, S.; Kotov, N. A. Direct-Write Maskless Lithography of LBL Nanocomposite Films and its Prospects for MEMS Technologies. *Nanoscale* **2012**, *4*, 4393−4398.

(8) Fuller, S.; Wilhelm, E.; Jacobson, J. Ink-Jet Printed Nanoparticle Microelectromechanical Systems. *J. Microelectromech. Syst.* **2002**, *11*, 54−60.

(9) Yokota, T.; Nakano, S.; Sekitani, T.; Someya, T. Plastic Complementary Microelectromechanical Switches. *Appl. Phys. Lett.* **2008**, *93*, 023305.

(10) Park, E. S.; Chen, Y.; Liu, T.-J. K.; Subramanian, V. A New Switching Device for Printed Electronics: Inkjet-Printed Microelectromechanical Relay. *Nano Lett.* **2013**, *13*, 5355−60.

(11) Jung, S.-H.; Chen, C.; Cha, S.-H.; Yeom, B.; Bahng, J. H.; Srivastava, S.; Zhu, J.; Yang, M.; Liu, S.; Kotov, N. A. Spontaneous Self-Organization Enables Dielectrophoresis of Small Nanoparticles and Formation of Photoconductive Microbridges. *J. Am. Chem. Soc.* **2011**, *133*, 10688−10691.

(12) Mueggenburg, K. E.; Lin, X.-M.; Goldsmith, R. H.; Jaeger, H. M. Elastic Membranes of Close-Packed Nanoparticle Arrays. *Nat. Mater.* **2007**, *6*, 656−660.

(13) He, J.; Kanjanaboos, P.; Frazer, N. L.; Weis, A.; Lin, X.-M.; Jaeger, H. M. Fabrication and Mechanical Properties of Large-Scale Freestanding Nanoparticle Membranes. *Small* **2010**, *6*, 1449−1456.

(14) Schlicke, H.; Leib, E. W.; Petrov, A.; Schröder, J. H.; Vossmeyer, T. Elastic and Viscoelastic Properties of Cross-Linked Gold Nanoparticles Probed by AFM Bulge Tests. *J. Phys. Chem. C* **2014**, *118*, 4386−4395.

(15) Jiang, C.; Markutsya, S.; Pikus, Y.; Tsukruk, V. V. Freely Suspended Nanocomposite Membranes as Highly Sensitive Sensors. *Nat. Mater.* **2004**, *3*, 721−728.

(16) Kanjanaboos, P.; Lin, X.-M.; Sader, J. E.; Rupich, S. M.; Jaeger, H. M.; Guest, J. R. Self-Assembled Nanoparticle Drumhead Resonators. *Nano Lett.* **2013**, *13*, 2158−62.

(17) Schlicke, H.; Schröder, J. H.; Trebbin, M.; Petrov, A.; Ijeh, M.; Weller, H.; Vossmeyer, T. Freestanding Films of Crosslinked Gold Nanoparticles Prepared via Layer-by-Layer Spin-Coating. *Nanotechnology* **2011**, *22*, 305303.

(18) Joseph, Y.; Besnard, I.; Rosenberger, M.; Guse, B.; Nothofer, H.-G.; Wessels, J. M.; Wild, U.; Knop-Gericke, A.; Su, D.; Schlögl, R.; Yasuda, A.; Vossmeyer, T. Self-Assembled Gold Nanoparticle/Alkanedithiol Films: Preparation, Electron Microscopy, XPS-Analysis, Charge Transport, and Vapor-Sensing Properties. *J. Phys. Chem. B* **2003**, *107*, 7406−7413.

(19) Brust, M.; Schiffrin, D. J.; Bethell, D.; Kiely, C. J. Novel Gold-Dithiol Nano-Networks with Non-Metallic Electronic Properties. *Adv. Mater.* **1995**, *7*, 795−797.

(20) Wessels, J. M.; Nothofer, H.-G.; Ford, W. E.; von Wrochem, F.; Scholz, F.; Vossmeyer, T.; Schroedter, A.; Weller, H.; Yasuda, A. Optical and Electrical Properties of Three-Dimensional Interlinked Gold Nanoparticle Assemblies. *J. Am. Chem. Soc.* **2004**, *126*, 3349−56.

(21) del Campo, A.; Greiner, C. SU-8: A Photoresist for High-Aspect-Ratio and 3D Submicron Lithography. *J. Micromech. Microeng.* **2007**, *17*, R81−R95.

(22) Conradie, E. H.; Moore, D. F. SU-8 Thick Photoresist Processing as a Functional Material for MEMS Applications. *J. Micromech. Microeng.* **2002**, *12*, 368−374.

(23) Small, M. K.; Nix, W. D. Analysis of the Accuracy of the Bulge Test in Determining the Mechanical Properties of Thin Films. *J. Mater. Res.* **1992**, *7*, 1553−1563.

(24) Olichwer, N.; Leib, E. W.; Halfar, A. H.; Petrov, A.; Vossmeyer, T. Cross-Linked Gold Nanoparticles on Polyethylene: Resistive Responses to Tensile Strain and Vapors. *ACS Appl. Mater. Interfaces* **2012**, *4*, 6151−6161.

(25) Vossmeyer, T.; Stolte, C.; Ijeh, M.; Kornowski, A.; Weller, H. Networked Gold-Nanoparticle Coatings on Polyethylene: Charge Transport and Strain Sensitivity. *Adv. Funct. Mater.* **2008**, *18*, 1611−1616.

(26) Herrmann, J.; Müller, K.-H.; Reda, T.; Baxter, G. R.; Raguse, B.; de Groot, G. J. J. B.; Chai, R.; Roberts, M.; Wieczorek, L. Nanoparticle Films as Sensitive Strain Gauges. *Appl. Phys. Lett.* **2007**, *91*, 183105.